CWE-8
June 7-11, 2026
London, ON, Canada

Effects of spanwise non-uniform inflow on the aerodynamic characteristics on a 5:1 rectangular cylinder

Pengxin Wang [a], Genshen Fang [b], Yaojun Ge [c]

[a]*Key Lab of Disaster Reduction in Civil Engineering, Tongji University, Shanghai 200092, China, 2211326@tongji.edu.cn*
[b]*Key Lab of Disaster Reduction in Civil Engineering, Tongji University, Shanghai 200092, China, 2222tjfgs@tongji.edu.cn*
[c]*Key Lab of Disaster Reduction in Civil Engineering, Tongji University, Shanghai 200092, China, yaojunge@tongji.edu.cn*

SUMMARY

Spanwise non-uniform inflows frequently occur in practice, and neglecting their effects may lead to non-conservative wind-resistant design for elongated structures. This study employs large eddy simulations (LES) to systematically examine how spanwise shear gradient in angle of attack (AoA) and inflow velocity modify the three-dimensional (3D) flow and aerodynamic responses of a 5:1 rectangular cylinder. After validation under uniform inflow, three AoA-shear and three velocity-shear cases are analyzed. Spanwise shear disrupts the coherence of separated vortices through section-to-section variations in separation and reattachment, leading to fragmented vortex topology, redistributed surface pressure, and reduced spanwise correlation. These changes weaken the periodic lift response and increase mean drag. Despite identical local inflow parameters, the mid-span section exhibits altered 2D flow patterns, including weakened or even split main vortex under AoA shear and earlier reattachment under velocity shear. The enlarged wake strengthens leeward suction, raising sectional mean drag by up to 19.7% and 21.1%.

Keywords: *Spanwise non-uniform inflow, 5:1 rectangular cylinder, Aerodynamic characteristics, LES*

1. INTRODUCTION

Flow around bluff bodies is a fundamental problem in fluid dynamics, yet most existing studies assume inflows with spatially uniform statistical characteristics, often even perfectly uniform. In practice, engineering inflows are far more complex: wind-speed profiles in the neutral atmospheric boundary layer (JTG/T 3360-01—2018, 2018), strong shear associated with non-synoptic winds such as typhoons and downbursts (Tamura et al., 2007; He et al., 2016), wind veering governed by the Coriolis force (Ekman, 1905), and spanwise non-uniform wind inflow induced by complex terrain (Lystad et al., 2018; Tang et al., 2020).

Existing research on spanwise velocity shear focuses predominantly on low Reynolds numbers, whereas real engineering applications generally fall within high-Reynolds-number regimes, limiting the applicability of current conclusions. Similarly, while some studies have considered wind veering effects, the underlying mechanisms by which spanwise AoA gradients affect flow structure evolution and aerodynamic forces are not well understood and lack systematic analysis. Moreover, although non-uniform inflow has been indicated to potentially degrade bridge aerodynamic stability, prior conclusions have not been supported by detailed CFD flow-field data to establish a clear cause-and-effect relationship between flow structures and aerodynamic responses. Additionally, the influence of spanwise shear gradients on the aerodynamics of local 2D cross sections has been largely overlooked, which could have implications for local damage.

Motivated by these gaps, this study conducts 3D LES of a 5:1 rectangular cylinder to investigate how spanwise variations in AoA and velocity modify flow structures and aerodynamics at high Reynolds numbers.

2. SIMULATION ARRANGEMENTS

In this study, a finite-span 5:1 rectangular cylinder is exposed to spanwise non-uniform inflows, including variations in AoA and wind velocity, as illustrated in Figure 1. To quantify these effects, two dimensionless parameters—the spanwise non-uniformity coefficients of AoA and velocity, denoted as α and β—are defined following the shear flow formulations used in previous studies (Cao et al., 2007; Zhao et al., 2023), as expressed in Eqs. (1) and (2). Three non-uniform AoA cases with α=1, 2, 3, and another three non-uniform velocity cases with β=0.04, 0.08, 0.12 are performed in this study. Averaged Re is set to 20000.

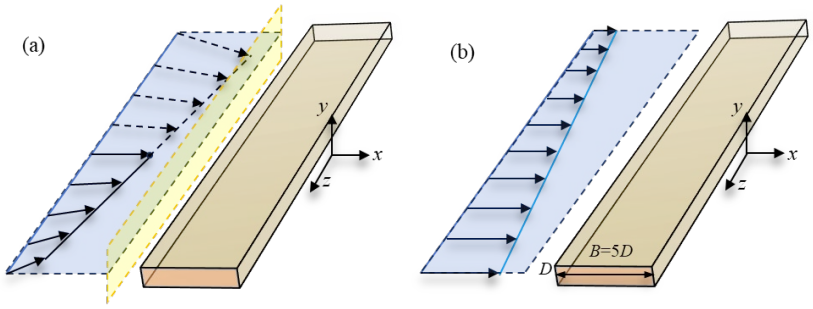

Figure 1: Spanwise non-uniformity of oncoming flow: (a) non-uniform AoA; (b) non-uniform wind velocity

$$\alpha = G_1 \times D = \frac{d\theta}{dz} \times D \tag{1}$$

$$\beta = G_2 \times \frac{D}{U_{ref}} = \frac{dU}{dz} \times \frac{D}{U_{ref}} \tag{2}$$

where G_1 and G_2 are the spanwise AoA and velocity gradient, which are the AoA increment $d\theta$ and velocity increment dU per dz along the spanwise direction; D represents the characteristic dimension of the structure, defined as the depth of the rectangular cylinder, and is set to 0.1 in this study; U_{ref} denotes the reference wind velocity, corresponding to the wind speed at the mid-span section in this study, and is set to 2 m/s.

Figure 2 shows the computational domain, boundary conditions, and the mesh system. The mesh system was generated using the snappyHexMesh utility in OpenFOAM, employing an octree-based adaptive refinement strategy that has been widely adopted in simulations of bluff-body flows. Spanwise mesh resolution is crucial for capturing 3D flows under non-uniform inflows (Zhang and Xu, 2020; Zou et al., 2022; Cao and Tamura, 2025). Unlike traditional uniform spanwise extrusion (Bruno et al., 2012; Patruno et al., 2016; Wu et al., 2020; Zhang et al., 2023), our octree refinement strategy efficiently varies spanwise resolution across zones. This maintains a highly refined surface grid (δz=1/64D, smaller than the limit (1/40D) recommended by Zhang and Xu, 2020) while avoiding excessive overall cell counts, totaling ~15.42 million cells per case.

For the boundary conditions, the no-slip wall condition is imposed on the cylinder surface. The inflow conditions are either uniform or spanwise non-uniform, while in all cases the inflow remains uniform in the lateral (y-) direction. An advective outflow boundary condition is applied at the outlet to prevent possible eddy reflections, and free-slip conditions are assigned to the top and bottom boundaries. Regarding the spanwise boundaries, the conventional periodic boundary conditions commonly used in simulations of infinitely long cylinders (Bruno et al., 2014; Zhang and Xu, 2020; Cao and Tamura, 2025) are no longer applicable because the spanwise non-uniform inflow would lead to a sawtooth-like velocity profile, making the simulation unphysical (Visakh et al., 2016). Instead, the free-slip boundary conditions imposed on the spanwise surfaces, as recommended by Lamballais and Silvestrini (2002), Silvestrini and Lamballais (2004), Visakh et al. (2016), and De and Sarkar (2020), allow the present simulation to effectively represent a finite-length rectangular cylinder. In fact, conducting numerical simulations of spanwise non-uniform inflows over an infinitely long cylinder is physically unrealistic.

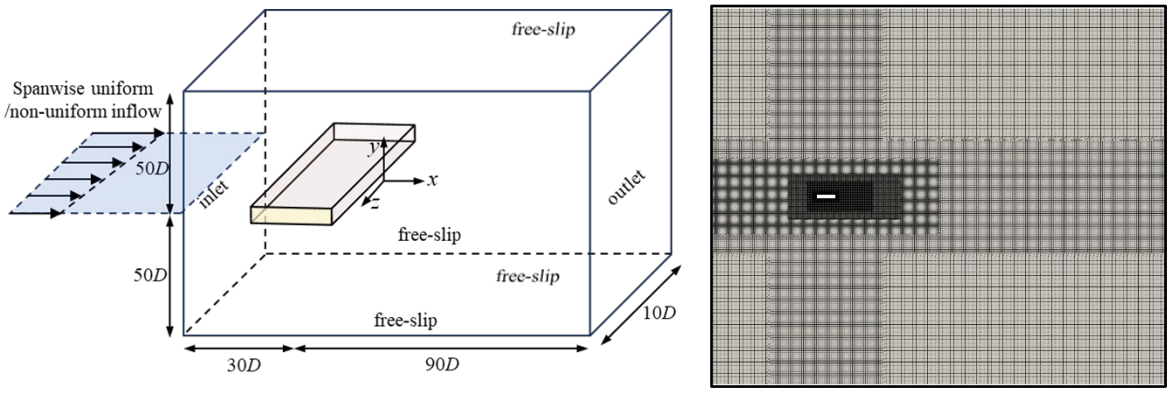

Figure 2: Computational domain, boundary conditions, and mesh system.

3. VALIDATIONS OF SIMULATION

To validate the numerical setup, Table 1 compares the predicted global aerodynamic parameters (mean drag coefficient C_D, RMS lift coefficient C_L', and Strouhal number St) of the 5:1 rectangular cylinder under uniform inflow with previous experimental and numerical studies. The computed C_D and St agree well with the reference data. Although literature values for the fluctuating lift coefficient exhibit considerable scatter—reflecting the inherent challenges of capturing high-Reynolds-number bluff body flows—our result falls well within the reported uncertainty range.

As shown in Figure 3(a), the present mean surface pressure agrees well with literature data. For the fluctuating pressure in Figure 3(b), despite the large scatter among previous studies, the present results match the reported magnitude and peak location, indicating acceptable accuracy. Remaining differences arise from the strong sensitivity of pressure fluctuations to factors such as Reynolds number, turbulence modeling, numerical schemes, and grid resolution. Notably, higher spanwise resolution reduces fluctuation levels (Zhang and Xu, 2020), consistent with our lower values compared with Zhang et al. (2023).

Table 1: Comparison of the aerodynamic parameters in uniform inflow conditions

References	$Re(10^4)$	Method	C_D	C_D'	St
Present study	2	LES	1.003	0.386	0.12
Bruno et al., 2012	4	LES	0.96-1.03	0.2-0.73	0.112-0.122
Mannini et al., 2017	2.3-11.2	WT	1.025-1.12	0.24-0.325	0.112-0.116
Zhang and Xu, 2020	4	LES	0.956-0.981	0.282-0.532	0.114-0.126
Li et al., 2020	1.3	WT	1.108	-	0.111
Zou et al., 2022	2.2	LES	0.99-1.274	0.484-1.012	0.1-0.16
Zhang et al., 2023	2	LES	0.98-0.997	0.381-0.416	0.108-0.112
Han et al., 2025	3.1-10.1	WT	1.11-1.15	-	0.087-0.094

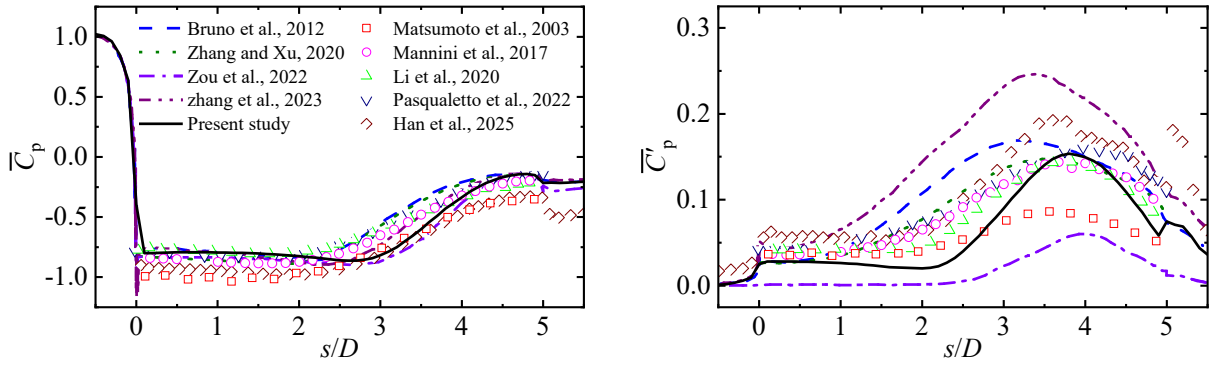

Figure 3: Comparison of the spanwise-averaged surface pressure distributions in uniform inflow: (a) mean pressure coefficient; (b) RMS pressure coefficient

4. RESULTS

Figure 4 illustrates the 3D flow structures (Q-criterion) around the 5:1 rectangular cylinder under uniform and spanwise non-uniform inflows at peak lift. Spanwise non-uniformity induces pronounced 3D variations, as separation and reattachment are highly sensitive to the AoA (Patruno et al., 2016; Wu et al., 2020; Han et al., 2025). Figure 4(a) shows that varying AoA causes coexisting fully separated ($z > 0$) and rapidly reattached ($z < 0$) flows. This contrast induces spanwise shear, stretching, and fragmenting vortex structures, thereby weakening their coherence and spanwise force correlation. Similarly, Figure 4(b) demonstrates that spanwise velocity shear also weakens vortex coherence. At the Reynolds number of 2×10^4, velocity gradients severely distort and tear vortex cores, disrupting the continuous oblique shedding observed in lower-Reynolds-number studies (Visakh et al., 2016). In summary, both spanwise AoA and velocity shear weaken vortex connectivity by creating differing separation behaviors along the span. The resulting fragmented topologies and their aerodynamic impacts are quantified in subsequent sections.

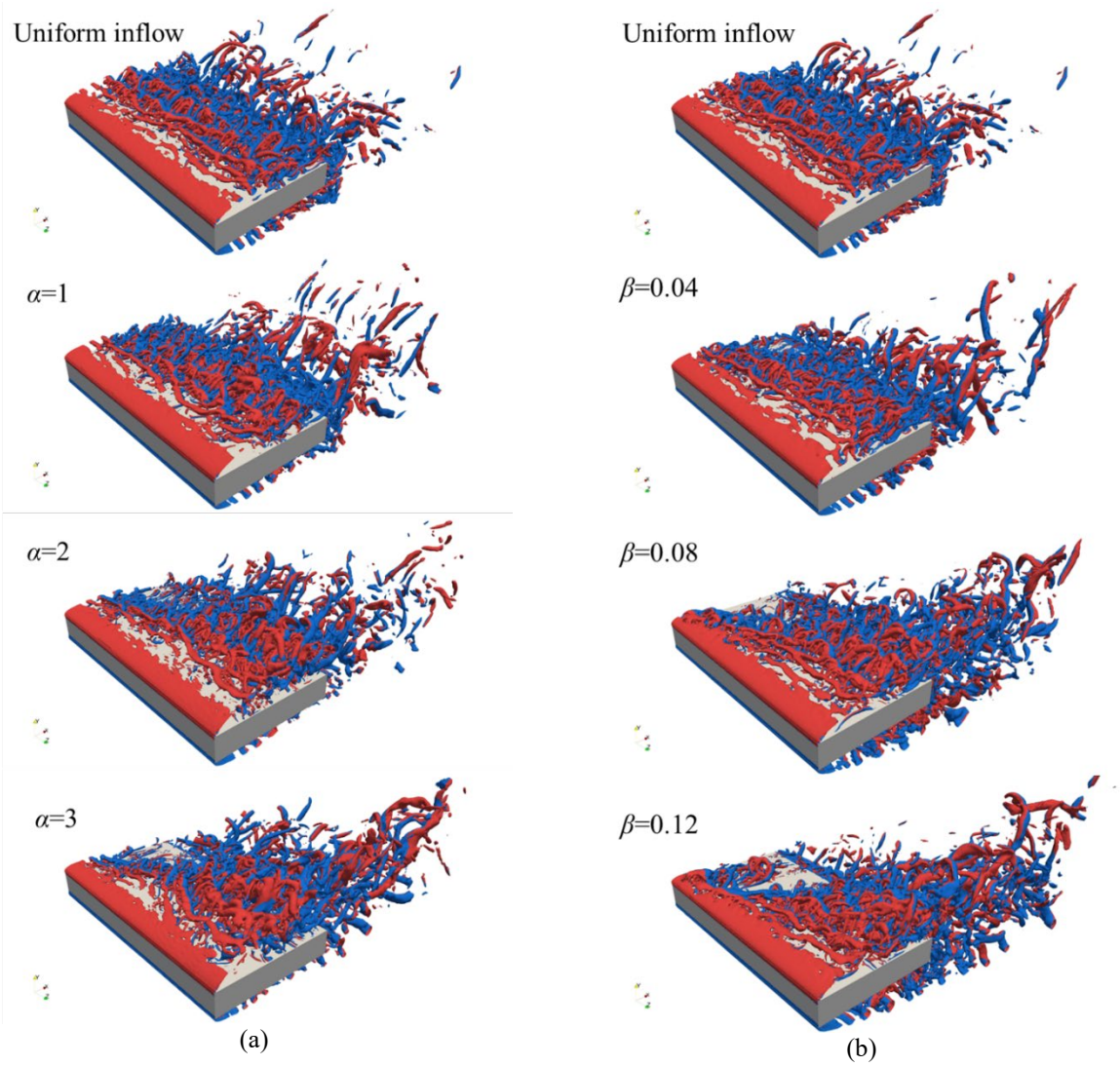

Figure 4: Topology of instantaneous vorticities at the instant of lift peak. The Q-criterion iso-surface ($Q = 2(U_{ref}/D)^2$) is colored by the sign of the y-direction velocity: (a) non-uniform AoA; (b) non-uniform velocity

As shown in Figure 5, the lift coefficient correlation weakens progressively as the parameter increases. Non-uniform velocity inflow reduces spanwise correlation faster than non-uniform AoA. Under strong velocity-shear, correlation drops to ~0.2 just 1D from mid-span before slightly recovering, reflecting complex 3D flow structures.

It is worth noting that the mid-span section consistently experiences a 2D uniform inflow (2 m/s, 0° AoA) across all 3D cases, differing only in the spanwise shear gradient. Figure 6 confirms this via symmetric time-averaged streamlines. The flow features three typical structures: the main separation vortex (characterized by reattachment length L_r via wall shear stress τ_{wall}), the secondary vortex, and the wake vortex (recirculation length L_w). Our uniform inflow results (L_r = 4.48D, L_w = 0.82D) validate well against previous literature (Zhang et al., 2023; Zou et al., 2022). The 3D shear significantly alters these characteristics (Figure 6b–c). Under non-uniform AoA inflow, L_r changes slightly, but the main vortex weakens. At high AoA shear, a dual-focus vortex emerges due to lost spanwise coherence and premature breakdown. Conversely, non-uniform

velocity inflow sharply decreases L_r (down to 3.31D at high shear) because the early 3D breakdown of the separated shear layer forces earlier reattachment. Regardless of the shear type, L_w increases with the shear gradient, as enhanced wake three-dimensionality broadens the mean reverse-flow region (Visakh et al., 2016). Overall, although the mid-span section experiences identical inflow velocity and AoA across all cases, the spanwise 3D shear significantly modifies its flow topology, which significantly affects the aerodynamic characteristics of the rectangular cylinder, as discussed in the following sections.

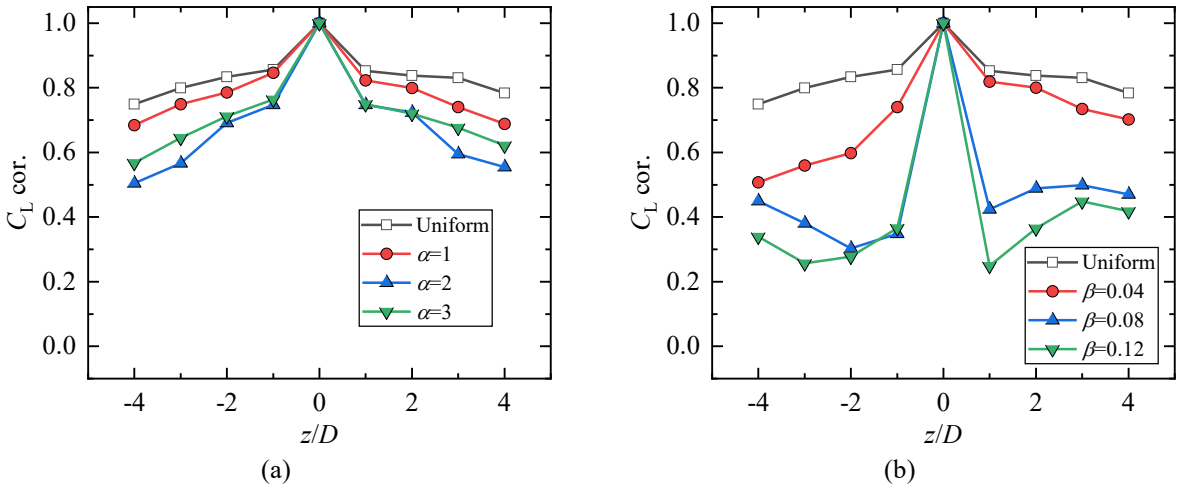

Figure 5: Spanwise correlation of lift coefficient in different inflow conditions: (a) non-uniform AoA; (b) non-uniform velocity

Figure 7 shows that spanwise shear significantly alters the mid-span 2D aerodynamic parameters. Increasing velocity or AoA shear gradients substantially raises the mean sectional drag coefficient by up to 19.7% and 21.1% relative to uniform inflow. This increase, driven by the enlarged wake vortex size (Figure 6), is crucial for local structural safety design. Conversely, the fluctuating drag coefficient remains nearly constant across all cases.

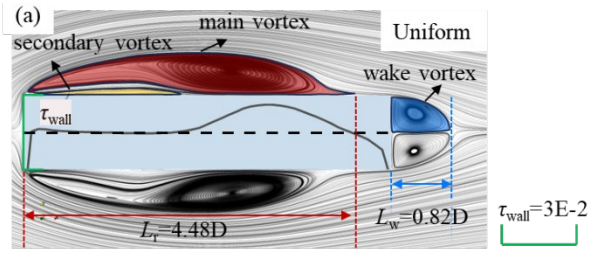

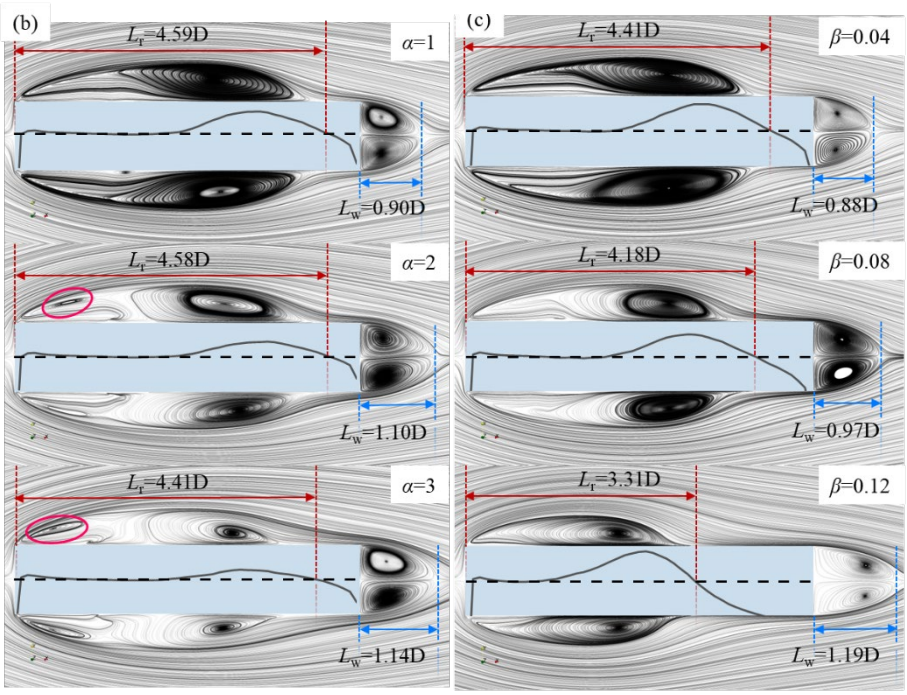

Figure 6: Time-averaged streamlines in the mid-span section under different inflow conditions: (a) uniform flow; (b) non-uniform AoA; (c) non-uniform velocity

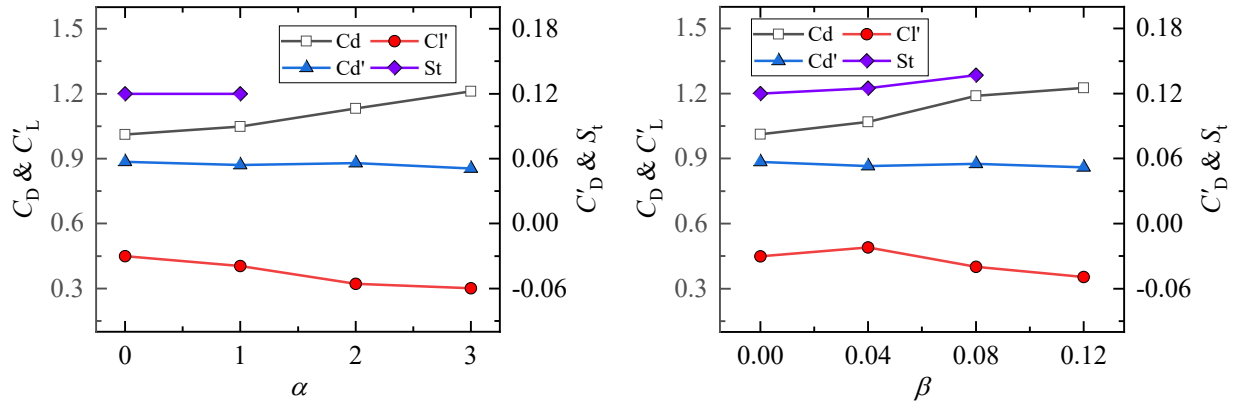

Figure 7: Sectional aerodynamic parameters in different inflow conditions: (a) non-uniform AoA; (b) non-uniform velocity

Aerodynamic force variations are governed by mean and fluctuating surface pressure distributions (Figure 8 and Figure 9). While 3D shear negligibly affects the windward surface, it lowers the mean leeward pressure. This enhanced suction explains the increased mean sectional drag observed in Figure 7. Side-surface pressures are highly sensitive to non-uniform inflows. Under increasing AoA shear, the minimum mean negative pressure at the leading edge rises, while trailing-edge negative pressure and peak fluctuating pressure both decrease, reflecting reduced

flow fluctuation energy. Conversely, non-uniform velocity inflow causes minor changes at low shear but significant effects at strong shear. Specifically, leading-edge minimum mean pressure drops, trailing-edge negative pressure rises, and the peak fluctuating pressure increase and shift upstream. This directly corresponds to the rapid early flow reattachment under strong velocity shear (Figure 6b).

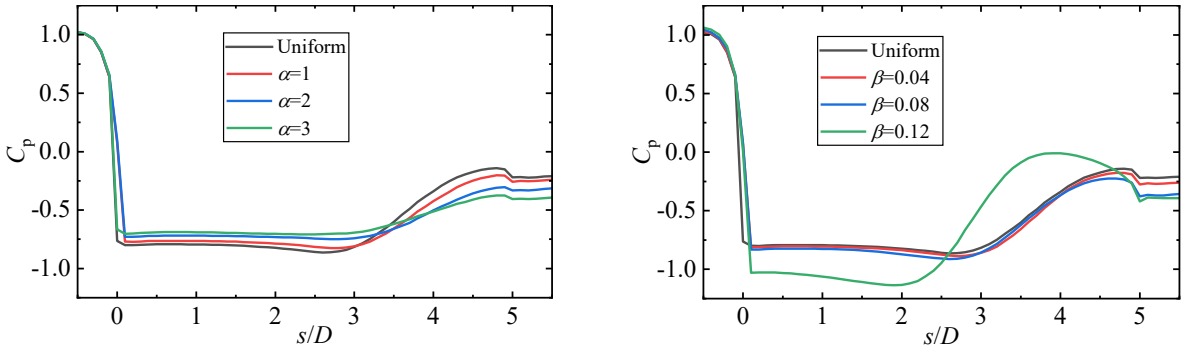

Figure 8: Comparison of the mean surface coefficient in mid span under different inflow conditions: (a) non-uniform AoA; (b) non-uniform velocity

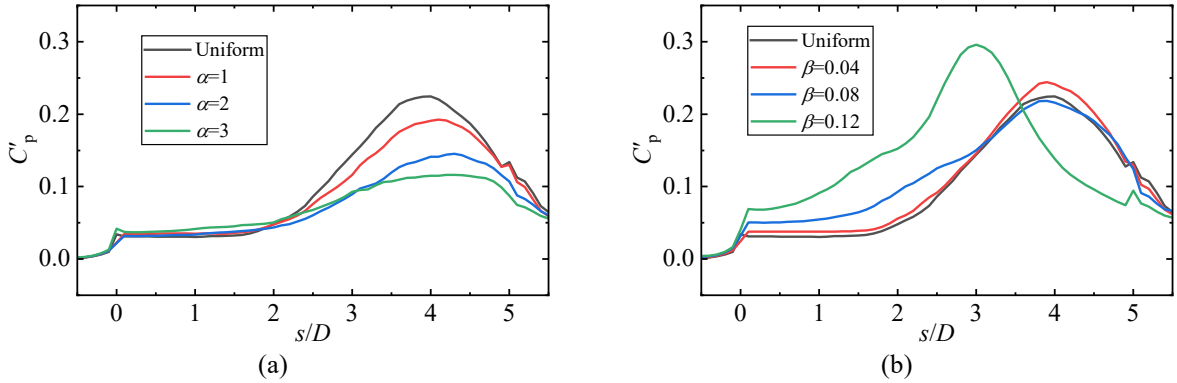

Figure 9: Comparison of the RMS surface coefficient in mid span under different inflow conditions: (a) non-uniform AoA; (b) non-uniform velocity

To elucidate 2D non-uniform inflow effects, Figure 10 presents side-surface streamwise pressure correlations (cross-correlated with a reference point at $s = 0.1D$). The uniform inflow results agree well with Wu et al. (2020), validating the simulation, while the slight deviations from Zhang et al. (2023) likely stem from our finer spanwise grid resolution. Mid-span fluctuating lift is primarily governed by pressure correlation at peak fluctuation locations. Under AoA shear, increasing gradients raise front-mid correlation but markedly decrease trailing-edge correlation, linking to the dual-focus vortex (Figure 6a). This reduced correlation, alongside diminished pressure amplitudes, decreases the fluctuating lift coefficient (Figure 7a). Conversely, high velocity shear sharply drops leading-edge correlation due to early vortex reattachment (Figure 6b). While increasing velocity shear generally decreases correlation at peak fluctuation points (Figure 10b), at a specific low shear gradient, slightly higher fluctuating pressure combined with mildly reduced correlation explains the minor increase in fluctuating lift (Figure 7b).

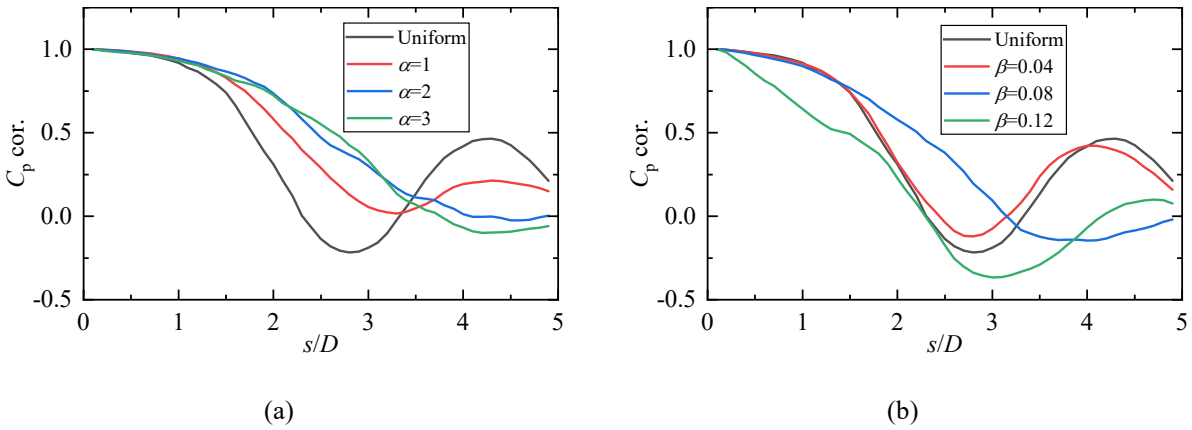

Figure 10: Surface pressure correlation in the streamwise direction under different inflow conditions: (a) non-uniform AoA; (b) non-uniform velocity

5. CONCLUSIONS

This study employs 3D LES to systematically examine how spanwise non-uniform inflows—characterized by spanwise gradients in AoA and inflow velocity—modify the 3D flow structures and aerodynamic responses of a 5:1 rectangular cylinder, with particular focus on the mid-span 2D section.

The results show that both AoA and velocity shear weaken the spanwise coherence of separated vortices due to variations in separation–reattachment behavior and separation rate among neighboring spanwise locations. The resulting fragmentation of vortex topology redistributes aerodynamic parameters along the span, reducing their correlation. Consequently, the global periodicity of the lift response is disrupted, and the fluctuating lift coefficient decreases with increasing shear intensity, while the modified 3D morphology leads to a marked increase in global mean drag. At the mid-span section, although the inflow sectional AoA and velocity remain unchanged across cases, spanwise shear substantially alters the intrinsic 2D flow pattern. Increasing AoA shear weakens the main vortex and even induces a dual-focus structure, whereas velocity shear reduces the side-vortex coherence and promotes earlier reattachment. These changes in flow topology explain the reduced fluctuating lift and the increased mean drag, with maximum drag increments of 19.7% and 21.1% under AoA and velocity shear, respectively.

The study provides quantitative insight into the mechanisms linking spanwise shear, flow evolution, and aerodynamic response, offering guidance for the wind-resistant design of structures in complex inflow environments.

ACKNOWLEDGEMENTS

The authors gratefully acknowledge the National Natural Science Foundation of China (52278520, 52578602, 52508578), Young Elite Scientists Sponsorship Program by CAST (2023QNRC001), Natural Science Foundation of Shanghai (25ZR1402494), the Committee of Science and Technology of Shanghai, China (24160712200).

REFERENCES

Bruno, L., Coste, N., Fransos, D., 2012. Simulated flow around a rectangular 5:1 cylinder: Spanwise discretisation ef fects and emerging flow features. J. Wind Eng. Ind. Aerod. 104-106, 203-215. https://doi.org/10.1016/j.jweia.2

012.03.018
Bruno, L., Salvetti, M.V., Ricciardelli, F., 2014. Benchmark on the aerodynamics of a rectangular 5: 1 cylinder: an o verview after the first four years of activity. J. Wind Eng. Ind. Aerod. 126, 87–106. https://doi.org/10.1016/j.jw eia.2014.01.005
Cao, S. Y., Ozono, S., Hirano, K., Tamura, Y., 2007. Vortex shedding and aerodynamic forces on a circular cylinder i n linear shear flow at subcritical Reynolds number. J. Fluids Struct. 23(5), 703-714. https://doi.org/10.1016/j.jf luidstructs.2006.11.004
Cao, Y., Tamura, T., 2025. Spanwise resolution effects on flow simulations around a square cylinder at the critical an gle. Phys. Fluids. 37, 095146. https://doi.org/10.1063/5.0289904
De, A. K., Sarkar, S., 2020. Wake events during early three-dimensional transition of a circular cylinder placed in she ar flow. Phys. Fluids. 32, 053603. https://doi.org/10.1063/1.5142258
Ekman, V.W., 1905. On the influence of the earth's rotation on ocean-currents. Arkiv fo ̈r Matematik, Astronomi och Fysik 2, 1–52.
Han, Y., Sun, Y. F., Liu, Q. K., Jing, H. M., Huang, H. J., Li, Z., Wang, Y. X., 2025. Aerodynamic characteristics of a 5:1 rectangular cylinder at Reynolds numbers of 3.12×105 to 1.01×106. Phys. Fluids. 37, 045121. https://doi.o rg/10.1063/5.0256739
He, Y. C., Chan, P. W., Li, Q. S., 2016. Observations of vertical wind profiles of tropical cyclones at coastal areas. J. Wind Eng. Ind. Aerod. 152, 1–14. http://dx.doi.org/10.1016/j.jweia.2016.01.009. https://doi.org/10.1016/j.jwei a.2016.01.009
JTG/T 3360-01—2018, 2018. Wind-resistant Design Specification for Highway Bridges. Ministry of Transport of th e People's Republic of China, Beijing, China.
Lamballais, E., Silvestrini, J. H., 2002. Direct numerical simulation of interactions between a mixing layer and a wak e around a cylinder. J. Turbul. 3, N28. 10.1088/1468-5248/3/1/028
Li, M., Li, Q., Shi, H., 2020. Aerodynamic pressures on a 5:1 rectangular cylinder in sinusoidal streamwise oscillator y flows with non-zero mean velocities. J. Wind Eng. Ind. Aerod. 208, 104440. https://doi.org/10.1016/j.jweia.2 020.104440
Lystad, T. M., Fenerci, A., Øiseth, O., 2018. Evaluation of mast measurements and wind tunnel terrain models to des cribe spatially variable wind field characteristics for long-span bridge design. J. Wind Eng. Ind. Aerod. 179, 55 8–573. https://doi.org/10.1016/j.jweia.2018.06.021
Mannini, C., Marra, A.M., Pigolotti, L., Bartoli, G., 2017. The effects of free-stream turbulence and angle of attack o n the aerodynamics of a cylinder with rectangular 5: 1 cross section. J. Wind Eng. Ind. Aerod. 161, 42–58. http s://doi.org/10.1016/j.jweia.2016.12.001
Patruno, L., Ricci, M., Miranda, S. de, Ubertini, F., 2016. Numerical simulation of a 5:1 rectangular cylinder at non-null angles of attack. J. Wind Eng. Ind. Aerod. 151, 146-157. https://doi.org/10.1016/j.jweia.2016.01.008
Silvestrini, J. H., Lamballais E., 2004. Direct numerical simulation of oblique vortex shedding from a cylinder in she ar flow. Int. J. Heat Fluid Flow. 25, 461. https://doi.org/10.1016/j.ijheatfluidflow.2004.02.013
Tamura, Y., Iwatani, Y., Hibi, K., Suda, K., Nakamura, O., Maruyama, T., Ishibashi, R., 2007. Profiles of mean wind speeds and vertical turbulence intensities measured at seashore and two inland sites using Doppler sodars. J. W ind Eng. Ind. Aerod. 95(6), 411–427. 10.1016/j.jweia.2006.08.005
Tang, H. J., Li, Y. L., Shum, K. M., Xu, X. Y., Tao, Q. Y., 2020. Non-uniform wind characteristics in mountainous ar eas and effects on flutter performance of a long-span suspension bridge. 201, 104177. https://doi.org/10.1016/j. jweia.2020.104177
Visakh, M. G., Saha, A. K., Muralidhar, K., 2016. Effect of spanwise shear on flow past a square cylinder at interme diate Reynolds numbers. Phys. Fluids. 28, 033602. 10.1063/1.4943975
Wu, B., Li, S. P., Li, K., Zhang, L. L., 2020. Numerical and experimental studies on the aerodynamics of a 5:1 rectan gular cylinder at angles of attack. J. Wind Eng. Ind. Aerod. 199, 104097. https://doi.org/10.1016/j.jweia.2020.1 04097
Zhang, Z. B., Xu, F. Y., 2020. Spanwise length and mesh resolution effects on simulated flow around a 5:1 rectangul ar cylinder. J. Wind Eng. Ind. Aerod. 202, 104186. https://doi.org/10.1016/j.jweia.2020.104186
Zhang, Y. X., Cao, S. Y., Cao, J. X., Wang, J., 2023. Effects of turbulence intensity and integral length scale on the su rface pressure on a rectangular 5:1 cylinder. J. Wind Eng. Ind. Aerod. 236, 105406. https://doi.org/10.1016/j.jw eia.2023.105406
Zhao, L., Xie, R. H., Huang, H. J., Yan, X. F., Cao, S. Y., Ge, Y. J., 2023. Aerodynamic characteristics of a streamline d box girder under shear flow considering oncoming turbulence. Phys. Fluids. 35, 095122. 10.1063/5.0147082
Zou, P. C., Cao, S. Y., Cao, J. X., 2022. Spanwise correlation and coherent structures of separated flow around rectan gular 5:1 cylinder. J. Wind Eng. Ind. Aerod. 231, 105211. https://doi.org/10.1016/j.jweia.2022.105211